

Supplementary Materials for

Molecular basis of JAK2 activation in erythropoietin receptor and pathogenic JAK2 signaling

Bobin George Abraham *et al.*

Corresponding author: Olli Silvennoinen, olli.silvennoinen@tuni.fi

Sci. Adv. **10**, eadl2097 (2024)
DOI: 10.1126/sciadv.adl2097

The PDF file includes:

Figs. S1 to S9
Tables S1 to S3
Legend for file S1
Reference

Other Supplementary Material for this manuscript includes the following:

File S1

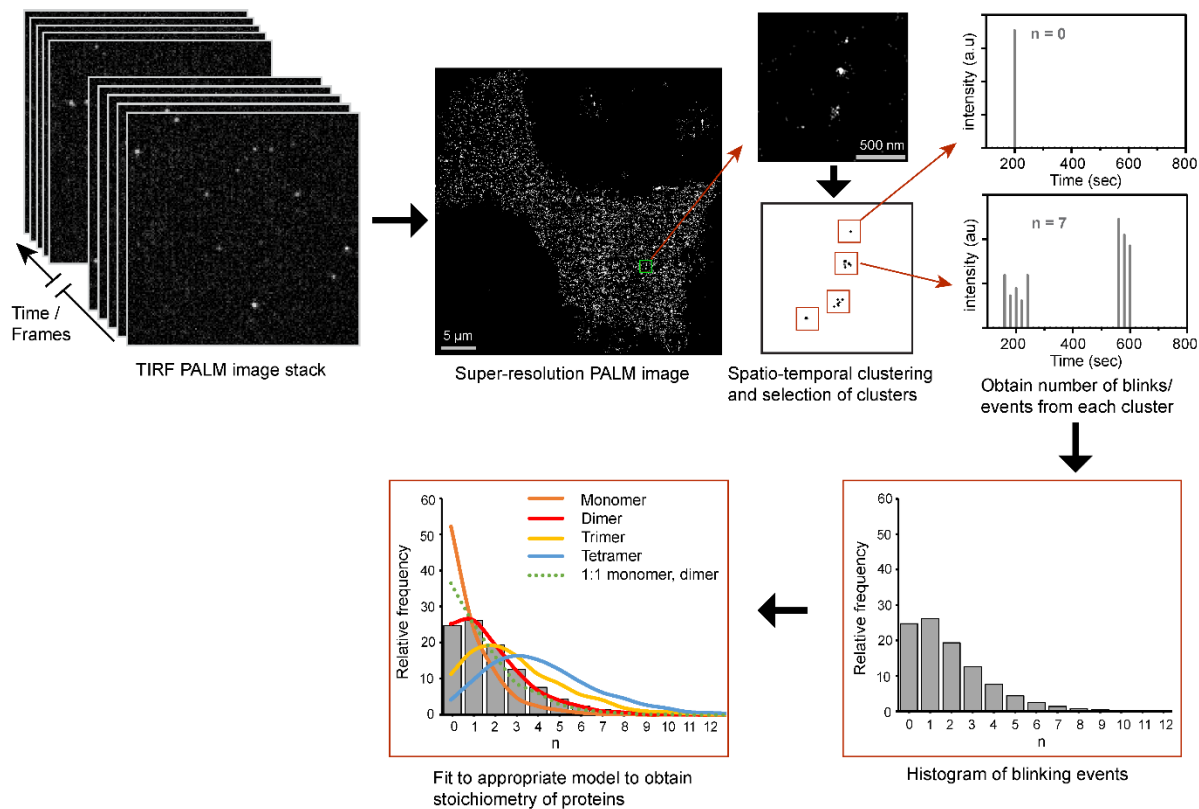


Fig. S1. qSMLM approach. From the time series TIRF PALM image stacks of the cell membrane expressing photoactivatable mEos3.2 fluorescent protein (top left), a super-resolved image (top middle) with localization data is generated. Individual clusters from the super-resolved image are selected and following spatio-temporal grouping, fluorescence bursts from individual cluster is extracted as a function of time (top right). The blinking events (fluorescence bursts minus one) from the clusters are plotted as a histogram (bottom right) to obtain the distribution of the blinking events. The distribution is then approximated with model functions to determine the oligomeric state of the proteins complex tagged with mEos3.2 (bottom left).

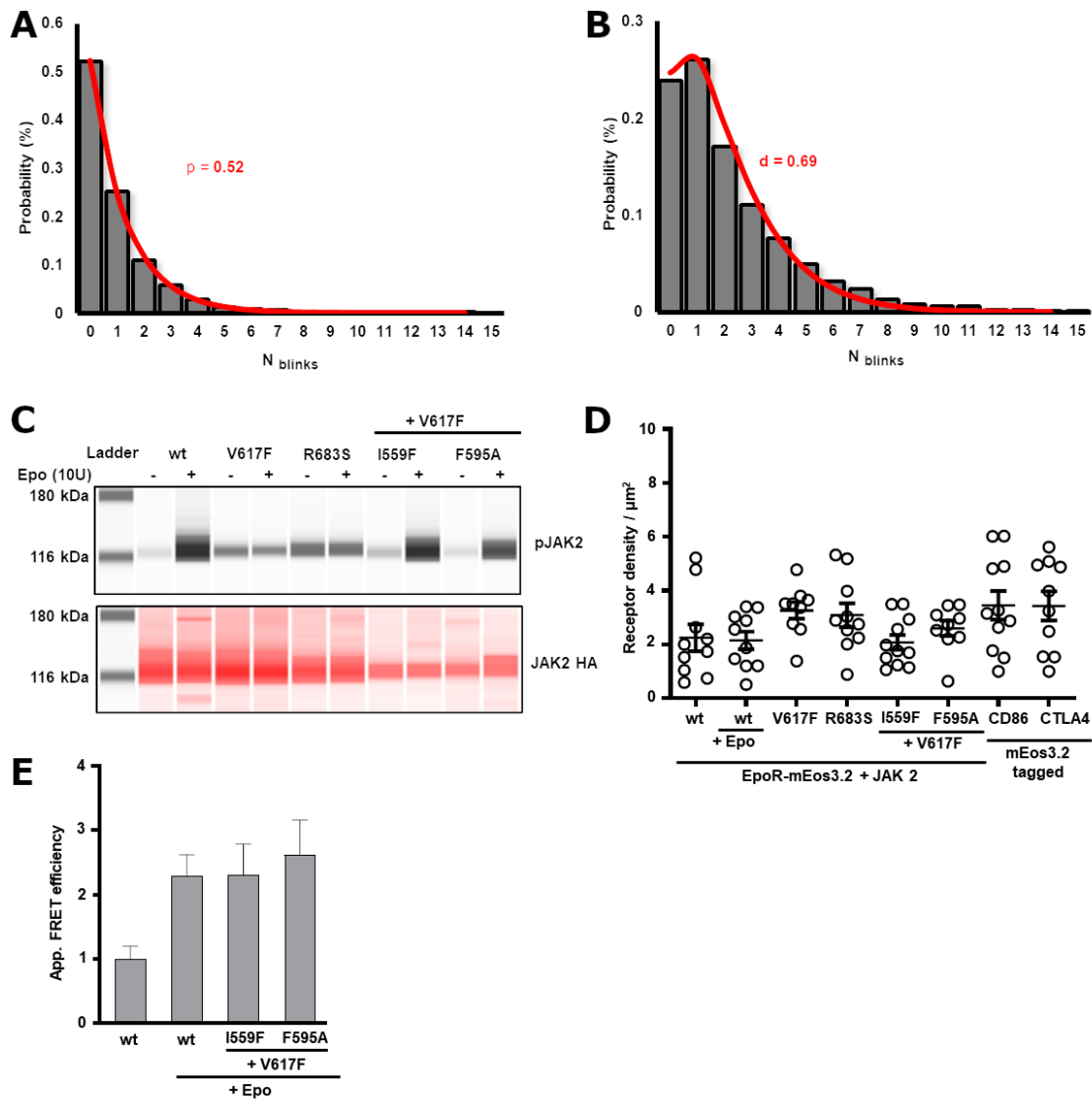


Fig. S2. Calibration of qSMLM. Analysis of the distribution of blinking events in γ 2A FlpIN TetON cell line stably expressing (A) the CD86 receptor (monomer control) and (B) CTLA4 (dimer control). By fitting the CD68 blink distribution, we calculated the parameter p that describes the fraction of molecules which did not blink ($p = 0.52$). The CTLA4 blink distribution was fitted according to a dimer fit function, resulting in the value $q = 0.31$ (fraction of undetected proteins) which translates to the detection efficiency of $d = 0.69$. (C) Capillary-based immunoblot showing JAK2 activation in Epo-induced stimulation in γ 2A cells stably expressing the EpoR-JAK constructs used in qSMLM. (D) Receptor density analyzed using the DBSCAN-based analysis from cells used for qSMLM analysis. Each data point represents the analysis from one cell with 10 cells measured for each condition. (E) FRET data showing enhanced EpoR dimerization upon Epo stimulation in both wildtype and V617F suppression mutants, suggesting restoration of wild-type behavior in these V617F suppression mutants. Error bar represents standard error and a minimum of 40 cells were analyzed for each condition.

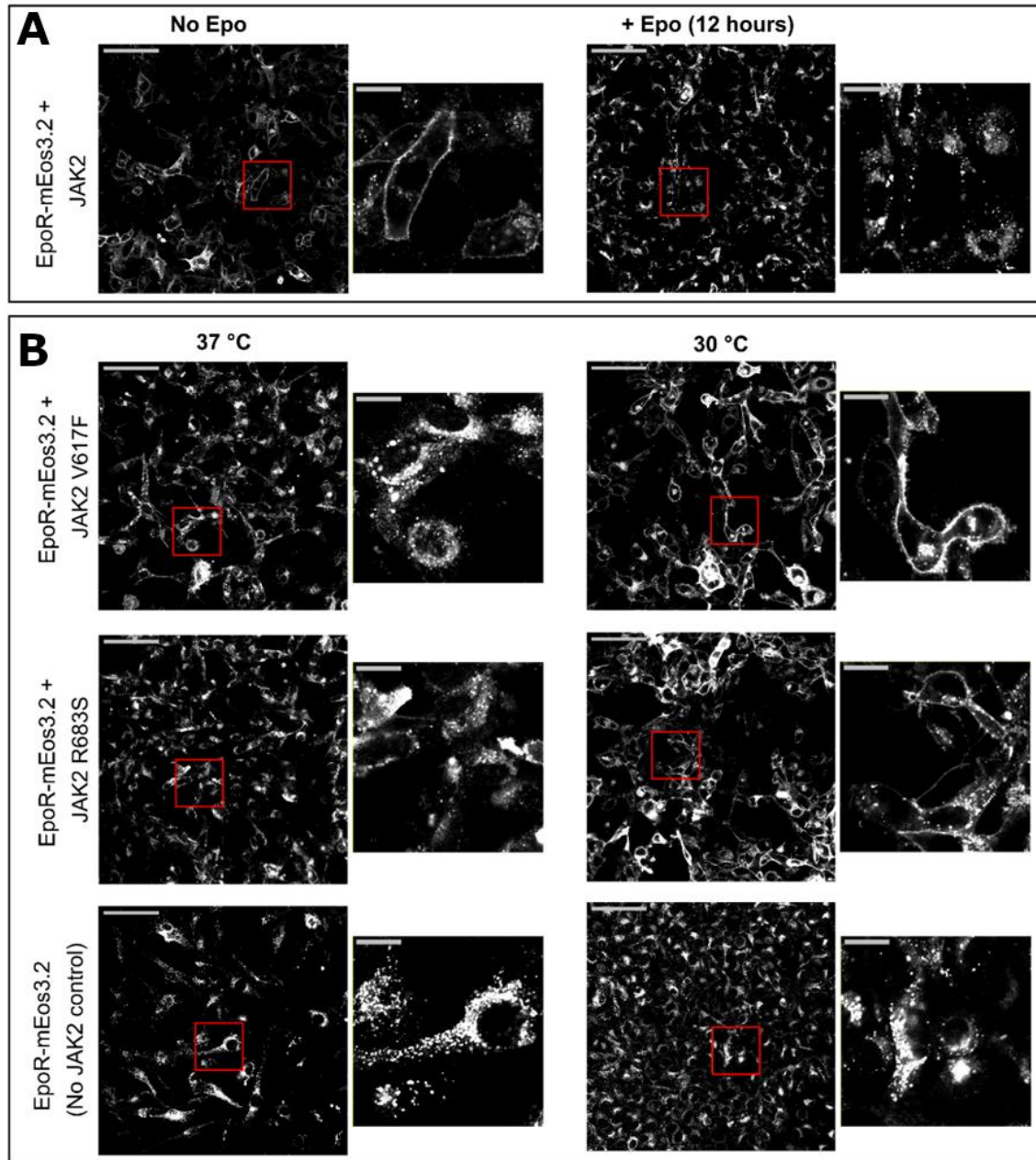


Fig. S3. Cell membrane localization of EpoR-mEos3.2 stably expressing in γ 2A FlpIn TetOn cells. (A) Lack of cell membrane expression, due to continuous internalization resulting from Epo stimulation, can be observed (the smaller image on the right-hand side is an inset from the boxed region). (B) Lack of membrane localization similar to Epo-stimulated cells can be observed with JAK2 constitutively active mutants (V617F and R683S) in normal culture conditions (37 °C). The membrane localization was restored in constitutively active mutants by culturing the cells at 30 °C after protein induction (images on the right side). Bottom image shows the lack of EpoR membrane localization in the absence of JAK2. As opposed to JAK2 activating mutants, the membrane expression is not restored in these cells even after culturing at 30 °C showing that JAK2 is necessary for EpoR membrane localization. (Scale 100 μ m, boxed region 20 μ m).

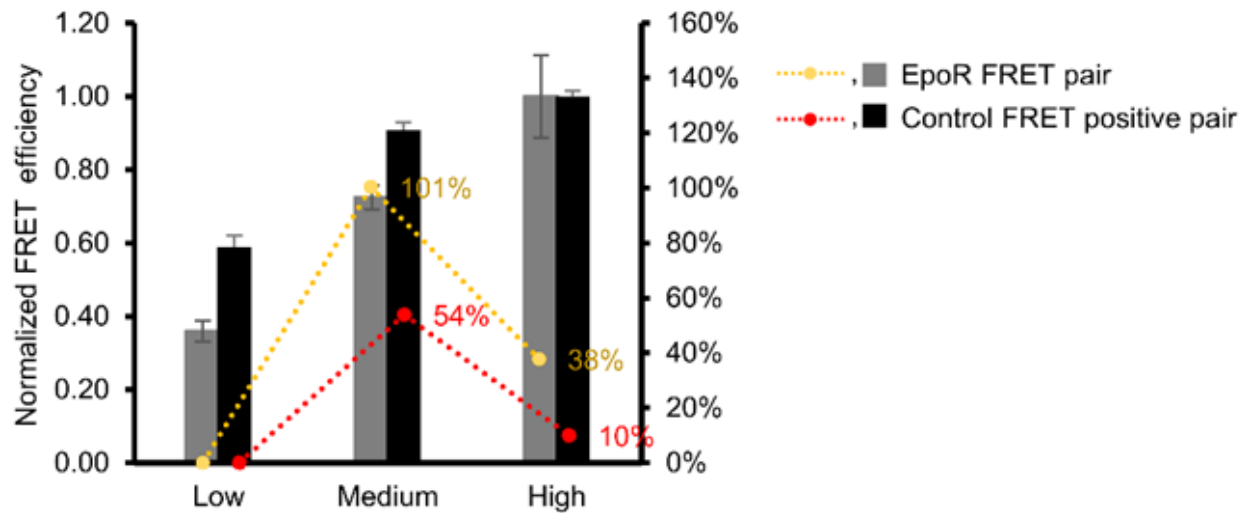


Fig. S4. Change in FRET with cells expressing different levels of EpoR FRET pair expression versus the control FRET positive FRET pair. The x-axis represents expression levels based on the YFP expression which is independent of FRET. Expression levels are normalized, where “Low” represents a fraction from 0 to 0.25, “Medium” is a fraction from 0.25 to 0.5, and “High” is a fraction from 0.5 to 1. The dotted lines represent the rate of change of FRET efficiency. An increased rate of changes can be observed in the EpoR FRET pair. The error bar represents standard error. A minimum of 10 cells were analyzed for each condition. The change in FRET response between different receptor expression levels was observed to be significantly higher than the change in FRET response of a control FRET pair. This indicated that the receptor undergoes dimerization on increasing the expression level and provided us with a confirmation that the response from FRET reporter is primarily due to the change in oligomerization level rather than from structural dynamics occurring in a pre-dimerized receptor/JAK2 complex. The increased FRET observed at higher EpoR/JAK2 expression levels indicated that the dimerization data obtained from higher receptor expression levels are due to overexpression-induced oligomerization and do not represent a physiological state of the cell. Therefore, we chose to restrict our analysis to cells expressing only low levels of receptor.

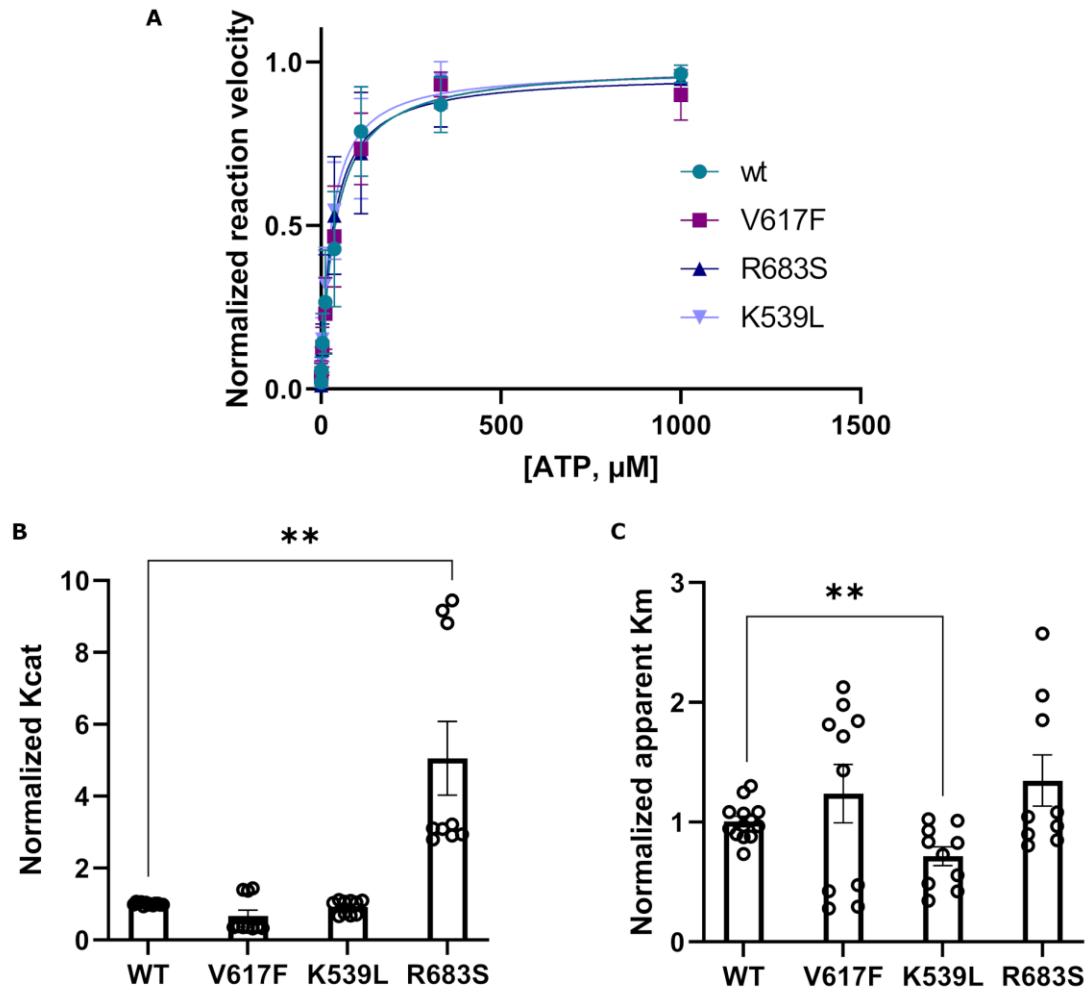


Fig. S5. R683S mutation affects the catalysis rate constant K_{cat} but not the ATP K_m . (A) Michaelis-Menten curves from kinase assay with ATP titration. Data presented are relative to maximum reaction velocity of WT. (B) Catalysis rate constant (K_{cat}) of mutants relative to WT calculated from ATP titrations. (C) The apparent K_m of mutants for ATP relative to WT. All data (A-C) is derived from 3 to 4 independent experiments and error bars represent the standard deviation (A) or standard error (B-C). Stars indicate statistical significance calculated using Welch's t test in comparison to WT: *, $p \leq 0.05$; **, $p \leq 0.01$; ***, $p \leq 0.001$; ****, $p < 0.0001$.

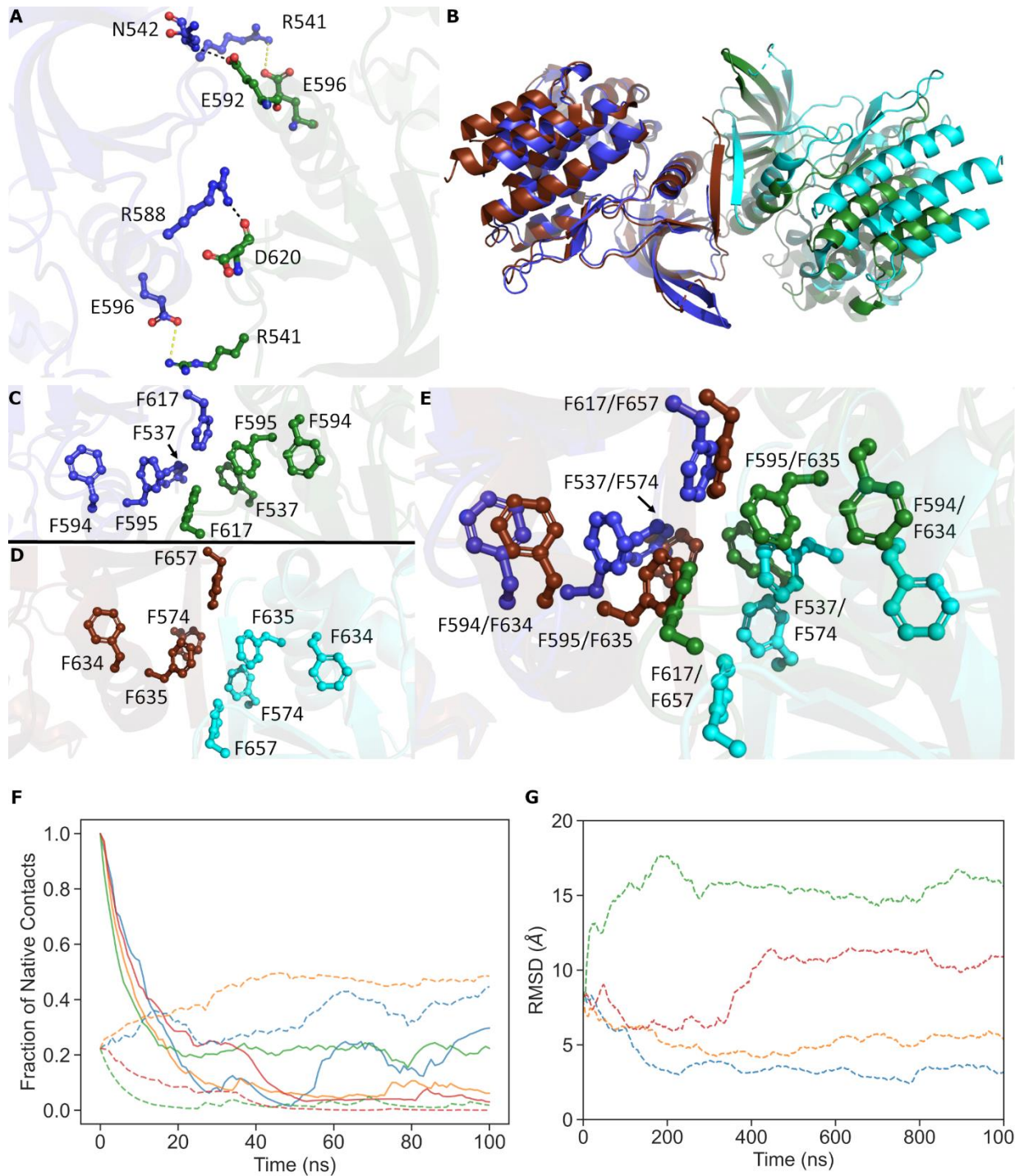


Fig. S6. JAK2 JH2 domain interface. (A) Stabilization of JAK2 JH2 V617F (PDB ID: 6D2I) interface by hydrogen bonding (black dotted lines) and salt bridges (yellow dotted lines). (B) Superposition of JAK2 JH2 V617F and JAK1 (PDB ID: 7T6F). Blue (JAK2) and brown (JAK1) monomers were superposed (RMSD = 1.375 Å for the aligned C α atoms). Differences in the dimer orientation can be seen from the non-aligned monomers across the interface (green and cyan for JAK2 and JAK1, respectively). (C) Aromatic stacking at the dimer interface of JAK2 JH2 V617F (PDB ID: 6D2I). (D) Dimer interface of JAK1 (PDB ID: 7T6F) displaying a looser packing of the interface. (E) Superposition of JAK2 JH2 and JAK1 JH2 dimers displays the tighter packing of

the interface in the JAK2 structure. **(F)** Time-resolved evolution of the fraction of native contacts in simulations of the K539L dimer. Native contacts (cutoff 4 Å) are heavy atom contacts between two monomeric chains of the dimer that are present in the reference crystal structures of V617F (solid lines) and K539L (dashed lines) variants. A value of 1.0 for the fraction of native contacts in V617F indicates 100% native contacts at the beginning of the simulation. The results of different simulation replicas are shown in different colors. **(G)** Root-mean-square deviation (RMSD) over all replicas as a function of simulation time for the K539L dimer variant with respect to the K539L dimer crystal structure used as the reference. Protein backbone RMSD over the trajectories was sampled every ns and presented as exponential moving averages with a 20 ns window. Replica trajectories are marked with different colors.

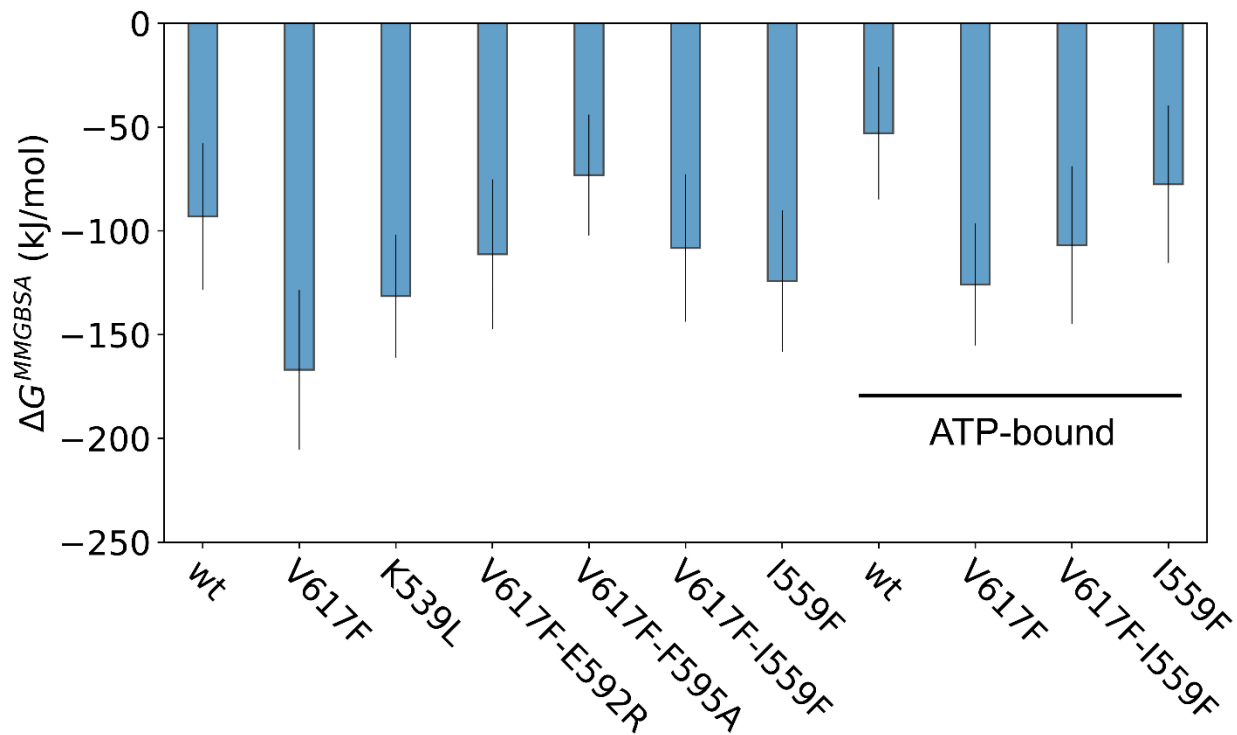


Fig. S7. Free-energy (ΔG^{MMGBSA}) values of JAK2 JH2 dimerization based on MMGBSA calculations. The data are presented for the ATP-free and ATP-bound (marked with “ATP-bound”) dimeric variants of JAK2 JH2. For details of the MMGBSA calculations, see Methods.

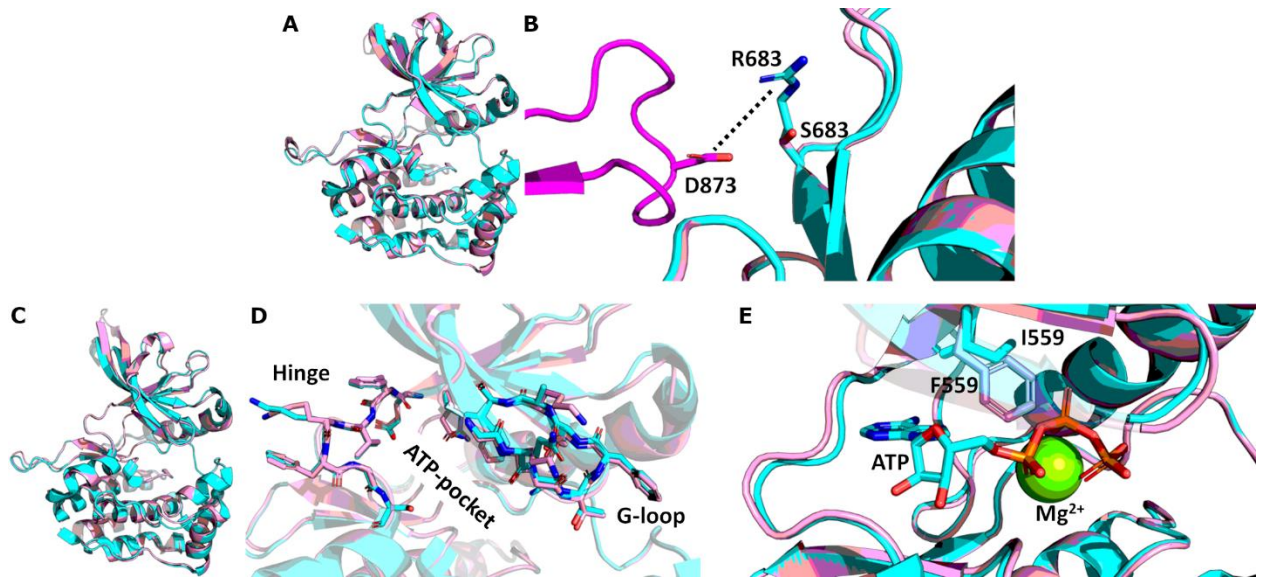


Fig. S8. Structural characterization of JAK2 R683S and I559F mutants. (A) Superposition of JAK2 JH2 R683S (pink) with JAK2 JH2 (cyan, PDB ID: 4fvp). No major structural changes are induced by the mutation. (B) JAK2 JH2 R683S / JAK2 JH2 and JAK2 JH1 (magenta) were superposed to the JH2 and JH1 domains of TYK2 structure (PDB ID: 4oli), respectively. The image shows the putative salt bridge (black dotted lines) between Asp873 of the JH1 domain and R683 of the wild-type JH2 domain. Mutation of R683 to G/S abolishes the interaction and destabilizes the autoinhibitory conformation. (C) Superposition of JAK2 JH2 I559F (pink) with JAK2 JH2 (cyan, PDB ID: 4fvp). No structural changes are induced by the mutation. (D) The figure shows the ATP pocket of JAK2 JH2. No structural changes are induced to the ATP-pocket by the I559F mutation when compared to the wild-type JAK2 JH2. (E) Superposition of JAK2 JH2 I559F (pink) with the JAK2 JH2 – ATP complex (cyan, PDB ID: 4fvq). The F559 mutant clashes with ATP, indicating that it is not competent in binding ATP.

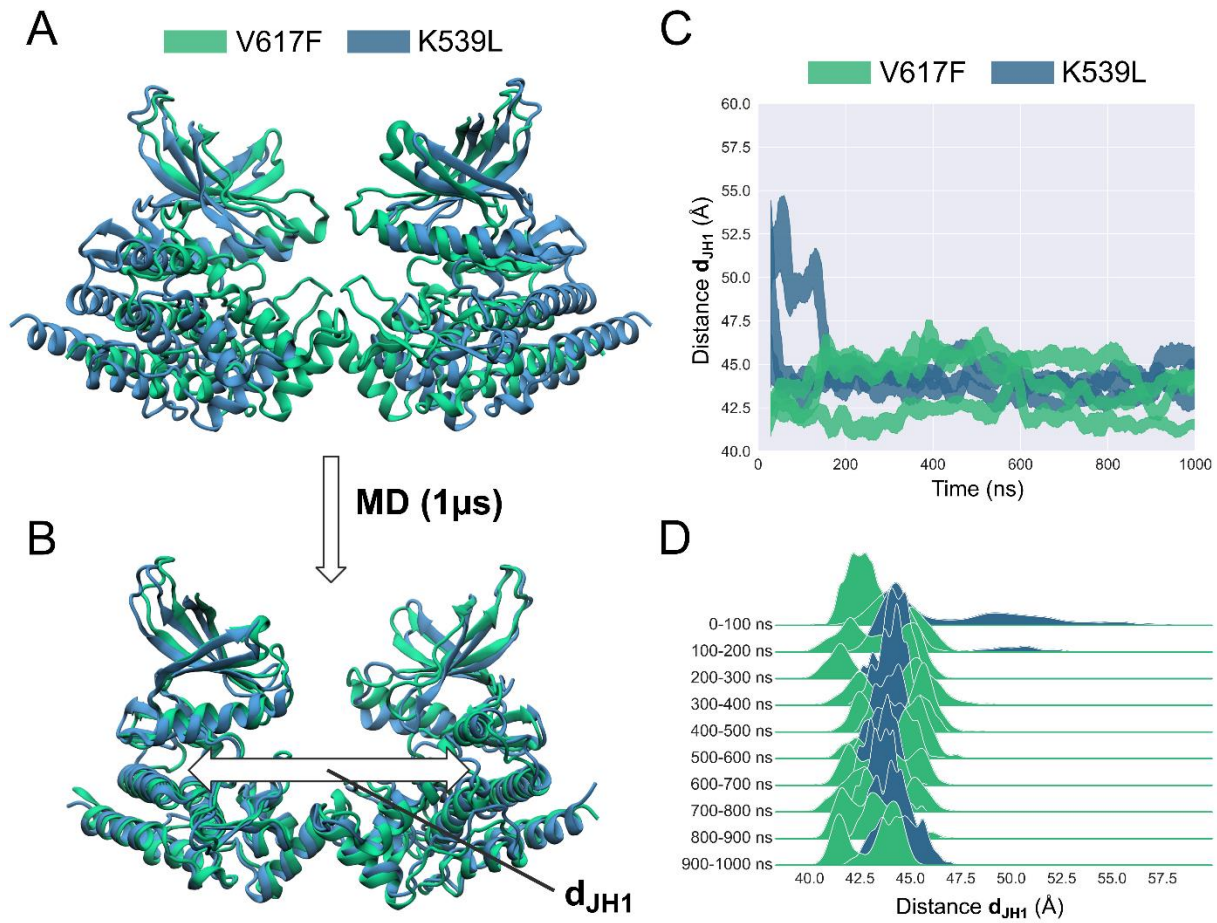


Fig. S9. Atomistic MD simulations of full-length AlphaFold2 models for JAK2-V617F and JAK2-K539L dimers. Panels (A) and (B) display snapshots of JH1 domains of JAK2-V617F and JAK2-K539L dimers captured at trajectory lengths of (A) 0 ns and (B) 1000 ns, respectively. The distance between the centers of mass for JH1 domains is denoted as d_{JH1} . (C) The distance d_{JH1} presented across all trajectories, with distance lines representing running means \pm running standard deviations. Panel (D) features the same information as panel (C) but displayed as a ridgeline density plot for specific time subsets of the simulation.

Table S1. Comparison of JAK2 V617F and K539L dimer interfaces. The analysis was performed with PDBsum (83).

Dimer	Chain	Interface area (Å)	Non-bonded contacts	Hydrogen bonds	Salt bridges
V617F	A	776	77	2	2
	B	781			
K539L	A	920	109	11	2
	B	827			

Table S2. Simulated systems.

System	Protein components (mutation, residue range, other information)	Water molecules and ions (K ⁺ , Cl ⁻)	# replicas/windows x duration (ns)	Type
FE1	JAK2 JH2/JH2 (wt, 536–808)	72979 (212, 208)	15 x 450	Free energy
FE2	JAK2 JH2/JH2 (V617F, 536–808)	72970 (212, 208)	15 x 450	Free energy
FE3	JAK2 JH2/JH2 (K539L, 536–808)	72976 (214, 208)	15 x 450	Free energy
FE4	JAK2 JH2/JH2 (V617F/F595A, 536–808)	72976 (212, 208)	15 x 450	Free energy
FE5	JAK2 JH2/JH2 (V617F/E592R, 536–808)	72967 (208, 208)	15 x 450	Free energy
EQ1	JAK2 JH2/JH2 (wt, 536–808)	74373 (215, 211)	4 x 1000	Equilibrium
EQ2	JAK2 JH2/JH2 (V617F, 536–808)	74316 (215, 211)	4 x 1000	Equilibrium
EQ3	JAK2 JH2/JH2 (K539L, 536–808)	74335 (217, 211)	4 x 1000	Equilibrium
EQ4	JAK2 JH2/JH2 (V617F/F595A, 536–808)	74318 (215, 211)	4 x 1000	Equilibrium
EQ5	JAK2 JH2/JH2 (V617F/E592R, 536–808)	74331 (211, 211)	4 x 1000	Equilibrium
EQ6	JAK2 JH2/JH2 (I559F, 536–808)	74322 (215, 211)	4 x 1000	Equilibrium
EQ7	JAK2 JH2/JH2 (V617F/I559F, 536–808)	74328 (215, 211)	4 x 1000	Equilibrium
EQ8	JAK2 JH2/JH2 ATP-bound (wt, 536–808)	71776 (218, 210)	3 x 1000	Equilibrium
EQ9	JAK2 JH2/JH2 ATP-bound (V617F, 536–808)	71763 (218, 210)	3 x 1000	Equilibrium
EQ10	JAK2 JH2/JH2 ATP-bound (I559F, 536–808)	71765 (218, 210)	3 x 1000	Equilibrium
EQ11	JAK2 JH2/JH2 ATP-bound (V617F/I559F, 536–808)	71762 (218, 210)	3 x 1000	Equilibrium
EQ12	JAK2 full-length dimer (V617F, 34–1132)	206860 (591, 587)	3 x 1000	Equilibrium
EQ13	JAK2 full-length dimer (K539L, 34–1132)	170707 (490, 484)	3 x 1000	Equilibrium

Table S3. Data collection and refinement statistics.

	JAK2 JH2-K539L (PDB code 8C08)	JAK2 JH2-R683S (PDB code 8C0A)	JAK2 JH2-I559F (PDB code 8C09)
Data			
Beam line	Diamond I03	Diamond I03	Diamond I03
Wavelength (Å)	0.97625	0.97625	0.97625
Space group	P4 ₃	P1	P2 ₁ 2 ₁ 2 ₁
Cell dimensions			
a, b, c (Å)	46.84, 46.84, 309.32	45.98, 56.69, 60.62	48.87, 53.19, 99.45
α, β, γ (°)	90.00, 90.00, 90.00	89.90, 79.58, 71.31	90.00, 90.00, 90.00
Resolution (Å)	77.37-2.20 (2.27-2.20)	59.51-1.70 (1.80-1.70)	53.19-1.90 (2.01-1.90)
CC _{1/2} (%)	0.999 (0.574)	0.997 (0.500)	0.997 (0.432)
I/σI	13.6 (1.2)	7.44 (1.07)	7.89 (0.84)
R _{merge}	0.141 (2.466)	0.057 (0.749)	0.182 (2.324)
Completeness (%)	100 (99.7)	95.0 (94.2)	100 (99.9)
Redundancy	14.2 (14.2)	1.8 (1.8)	6.4 (6.6)
Refinement			
Reflections	33587	119304	39505
R _{work} /R _{free}	0.230/ 0.259	0.194/0.238	0.221/0.257
RMSD of bond lengths (Å)	0.002	0.020	0.004
RMSD of bond angles (°)	0.515	1.523	0.526
B-factors (Å ²)			
Protein	56.67	30.58	38.80
Waters	51.40	35.78	39.39

Values for the highest-resolution shell are shown in parentheses.

File S1: MD simulation models. Initial and final system coordinates.

REFERENCES AND NOTES

1. H. M. Hammarén, A. T. Virtanen, J. Raivola, O. Silvennoinen, The regulation of JAKs in cytokine signaling and its breakdown in disease. *Cytokine* **118**, 48–63 (2019).
2. R. L. Philips, Y. Wang, H. Cheon, Y. Kanno, M. Gadina, V. Sartorelli, C. M. Horvath, J. E. Darnell, G. R. Stark, J. J. O’Shea, The JAK-STAT pathway at 30: Much learned, much more to do. *Cell* **185**, 3857–3876 (2022).
3. B. A. Witthuhn, F. W. Quelle, O. Silvennoinen, T. Yi, B. Tang, O. Miura, J. N. Ihle, JAK2 associates with the erythropoietin receptor and is tyrosine phosphorylated and activated following stimulation with erythropoietin. *Cell* **74**, 227–236 (1993).
4. E. Parganas, D. Wang, D. Stravopodis, D. J. Topham, J.-C. Marine, S. Teglund, E. F. Vanin, S. Bodner, O. R. Colamonici, J. M. van Deursen, G. Grosveld, J. N. Ihle, Jak2 is essential for signaling through a variety of cytokine receptors. *Cell* **93**, 385–395 (1998).
5. R. J. Brown, J. J. Adams, R. A. Pelekanos, Y. Wan, W. J. McKinstry, K. Palethorpe, R. M. Seeber, T. A. Monks, K. A. Eidne, M. W. Parker, M. J. Waters, Model for growth hormone receptor activation based on subunit rotation within a receptor dimer. *Nat. Struct. Mol. Biol.* **12**, 814–821 (2005).
6. A. de la Chapelle, A. L. Träskelin, E. Juvonen, Truncated erythropoietin receptor causes dominantly inherited benign human erythrocytosis. *Proc. Natl. Acad. Sci. U.S.A.* **90**, 4495–4499 (1993).
7. S. S. Watowich, The erythropoietin receptor: Molecular structure and hematopoietic signaling pathways. *J. Invest. Med.* **59**, 1067–1072 (2011).
8. O. Silvennoinen, S. R. Hubbard, Molecular insights into regulation of JAK2 in myeloproliferative neoplasms. *Blood* **125**, 3388–3392 (2015).

9. E. J. Baxter, L. M. Scott, P. J. Campbell, C. East, N. Fourouclas, S. Swanton, G. S. Vassiliou, A. J. Bench, E. M. Boyd, N. Curtin, M. A. Scott, W. N. Erber, A. R. Green, Acquired mutation of the tyrosine kinase JAK2 in human myeloproliferative disorders. *Lancet* **365**, 1054–1061 (2005).
10. C. James, V. Ugo, J.-P. Le Couédic, J. Staerk, F. Delhommeau, C. Lacout, L. Garçon, H. Raslova, R. Berger, A. Bennaceur-Griscelli, J. L. Villevalet, S. N. Constantinescu, N. Casadevall, W. Vainchenker, A unique clonal JAK2 mutation leading to constitutive signalling causes polycythaemia vera. *Nature* **434**, 1144–1148 (2005).
11. R. Kralovics, F. Passamonti, A. S. Buser, S.-S. Teo, R. Tiedt, J. R. Passweg, A. Tichelli, M. Cazzola, R. C. Skoda, A gain-of-function mutation of JAK2 in myeloproliferative disorders. *N. Engl. J. Med.* **352**, 1779–1790 (2005).
12. R. L. Levine, M. Wadleigh, J. Cools, B. L. Ebert, G. Wernig, B. J. P. Huntly, T. J. Boggan, I. Wlodarska, J. J. Clark, S. Moore, J. Adelsperger, S. Koo, J. C. Lee, S. Gabriel, T. Mercher, A. D’Andrea, S. Fröhling, K. Döhner, P. Marynen, P. Vandenberghe, R. A. Mesa, A. Tefferi, J. D. Griffin, M. J. Eck, W. R. Sellers, M. Meyerson, T. R. Golub, S. J. Lee, D. G. Gilliland, Activating mutation in the tyrosine kinase JAK2 in polycythemia vera, essential thrombocythemia, and myeloid metaplasia with myelofibrosis. *Cancer Cell* **7**, 387–397 (2005).
13. L. M. Scott, W. Tong, R. L. Levine, M. A. Scott, P. A. Beer, M. R. Stratton, P. A. Futreal, W. N. Erber, M. F. McMullin, C. N. Harrison, A. J. Warren, D. G. Gilliland, H. F. Lodish, A. R. Green, JAK2 exon 12 mutations in polycythemia vera and idiopathic erythrocytosis. *N. Engl. J. Med.* **356**, 459–468 (2007).
14. D. Bercovich, I. Ganmore, L. M. Scott, G. Wainreb, Y. Birger, A. Elimelech, C. Shochat, G. Cazzaniga, A. Biondi, G. Basso, G. Cario, M. Schrappe, M. Stanulla, S. Strehl, O. A. Haas, G. Mann, V. Binder, A. Borkhardt, H. Kempfki, J. Trka, B. Bielorei, S. Avigad, B. Stark, O. Smith, N. Dastugue, J.-P. Bourquin, N. B. Tal, A. R. Green, S. Izraeli, Mutations of JAK2 in acute lymphoblastic leukaemias associated with Down’s syndrome. *Lancet* **372**, 1484–1492 (2008).
15. G. Carreño-Tarragona, L. N. Varghese, E. Sebastián, E. Gálvez, A. Marín-Sánchez, N. López-Muñoz, S. Nam-Cha, J. Martínez-López, S. N. Constantinescu, J. Sevilla, R. Ayala, A typical

acute lymphoblastic leukemia JAK2 variant, R683G, causes an aggressive form of familial thrombocytosis when germline. *Leukemia* **35**, 3295–3298 (2021).

16. P. Saharinen, K. Takaluoma, O. Silvennoinen, Regulation of the Jak2 tyrosine kinase by its pseudokinase domain. *Mol. Cell. Biol.* **20**, 3387–3395 (2000).
17. P. Saharinen, O. Silvennoinen, The pseudokinase domain is required for suppression of basal activity of Jak2 and Jak3 tyrosine kinases and for cytokine-inducible activation of signal transduction. *J. Biol. Chem.* **277**, 47954–47963 (2002).
18. P. Saharinen, M. Vihinen, O. Silvennoinen, Autoinhibition of Jak2 tyrosine kinase is dependent on specific regions in its pseudokinase domain. *Mol. Biol. Cell* **14**, 1448–1459 (2003).
19. Y. Shan, K. Gnanasambandan, D. Ungureanu, E. T. Kim, H. Hammarén, K. Yamashita, O. Silvennoinen, D. E. Shaw, S. R. Hubbard, Molecular basis for pseudokinase-dependent autoinhibition of JAK2 tyrosine kinase. *Nat. Struct. Mol. Biol.* **21**, 579–584 (2014).
20. P. J. Lupardus, M. Ultsch, H. Wallweber, P. Bir Kohli, A. R. Johnson, C. Eigenbrot, Structure of the pseudokinase–kinase domains from protein kinase TYK2 reveals a mechanism for Janus kinase (JAK) autoinhibition. *Proc. Natl. Acad. Sci. U.S.A.* **111**, 8025–8030 (2014).
21. S. Wilmes, M. Hafer, J. Vuorio, J. A. Tucker, H. Winkelmann, S. Löchte, T. A. Stanly, K. D. Pulgar Prieto, C. Poojari, V. Sharma, C. P. Richter, R. Kurre, S. R. Hubbard, K. C. Garcia, I. Moraga, I. Vattulainen, I. S. Hitchcock, J. Piehler, Mechanism of homodimeric cytokine receptor activation and dysregulation by oncogenic mutations. *Science* **367**, 643–652 (2020).
22. E. Leroy, T. Balligand, C. Pecquet, C. Mouton, D. Colau, A. K. Shiao, A. Dusa, S. N. Constantinescu, Differential effect of inhibitory strategies of the V617 mutant of JAK2 on cytokine receptor signaling. *J. Allergy Clin. Immunol.* **144**, 224–235 (2019).
23. H. M. Hammarén, A. T. Virtanen, B. G. Abraham, H. Peussa, S. R. Hubbard, O. Silvennoinen, Janus kinase 2 activation mechanisms revealed by analysis of suppressing mutations. *J. Allergy Clin. Immunol.* **143**, 1549–1559.e6 (2019).

24. C. R. Glassman, N. Tsutsumi, R. A. Saxton, P. J. Lupardus, K. M. Jude, K. C. Garcia, Structure of a Janus kinase cytokine receptor complex reveals the basis for dimeric activation. *Science* **376**, 163–169 (2022).
25. N. A. Caveney, R. A. Saxton, D. Waghray, C. R. Glassman, N. Tsutsumi, S. R. Hubbard, K. C. Garcia, Structural basis of Janus kinase trans-activation. *Cell Rep.* **42**, 112201 (2023).
26. J. Staerk, A. Kallin, J.-B. Demoulin, W. Vainchenker, S. N. Constantinescu, JAK1 and Tyk2 activation by the Homologous Polycythemia Vera JAK2 V617F mutation: Cross-talk with IGF1 receptor . *J. Biol. Chem.* **280**, 41893–41899 (2005).
27. C. Karathanasis, J. Medler, F. Fricke, S. Smith, S. Malkusch, D. Widera, S. Fulda, H. Wajant, S. J. L. van Wijk, I. Dikic, M. Heilemann, Single-molecule imaging reveals the oligomeric state of functional TNF α -induced plasma membrane TNFR1 clusters in cells. *Sci. Signal.* **13**, eaax5647 (2020).
28. F. Fricke, J. Beaudouin, R. Eils, M. Heilemann, One, two or three? Probing the stoichiometry of membrane proteins by single-molecule localization microscopy. *Sci. Rep.* **5**, 14072 (2015).
29. C. L. Krüger, M.-T. Zeuner, G. S. Cottrell, D. Widera, M. Heilemann, Quantitative single-molecule imaging of TLR4 reveals ligand-specific receptor dimerization. *Sci. Signal.* **10**, eaan1308 (2017).
30. R. S. Kasai, S. V. Ito, R. M. Awane, T. K. Fujiwara, A. Kusumi, The class-A GPCR dopamine D2 receptor forms transient dimers stabilized by agonists: Detection by single-molecule tracking. *Cell Biochem. Biophys.* **76**, 29–37 (2018).
31. L. Salavessa, T. Lagache, V. Malardé, A. Grassart, J.-C. Olivo-Marin, A. Canette, M. Trichet, P. J. Sansonetti, N. Sauvonnet, Cytokine receptor cluster size impacts its endocytosis and signaling. *Proc. Natl. Acad. Sci. U.S.A.* **118**, e2024893118 (2021).
32. L. J. Huang, S. N. Constantinescu, H. F. Lodish, The N-terminal domain of Janus kinase 2 is required for Golgi processing and cell surface expression of erythropoietin receptor. *Mol. Cell* **8**, 1327–1338 (2001).

33. F. Passamonti, C. Elena, S. Schnittger, R. C. Skoda, A. R. Green, F. Girodon, J.-J. Kiladjian, M. F. McMullin, M. Ruggeri, C. Besses, A. M. Vannucchi, E. Lippert, H. Gisslinger, E. Rumi, T. Lehmann, C. A. Ortmann, D. Pietra, C. Pascutto, T. Haferlach, M. Cazzola, Molecular and clinical features of the myeloproliferative neoplasm associated with JAK2 exon 12 mutations. *Blood* **117**, 2813–2816 (2011).
34. R. Andraos, Z. Qian, D. Bonenfant, J. Rubert, E. Vangrevelinghe, C. Scheufler, F. Marque, C. H. Régnier, A. D. Pover, H. Ryckelynck, N. Bhagwat, P. Koppikar, A. Goel, L. Wyder, G. Tavares, F. Baffert, C. Pissot-Soldermann, P. W. Manley, C. Gaul, H. Voshol, R. L. Levine, W. R. Sellers, F. Hofmann, T. Radimerski, Modulation of activation-loop phosphorylation by JAK inhibitors is binding mode dependent. *Cancer Discov.* **2**, 512–523 (2012).
35. E. Leroy, A. Dusa, D. Colau, A. Motamedi, X. Cahu, C. Mouton, L. J. Huang, A. K. Shiao, S. N. Constantinescu, Uncoupling JAK2 V617F activation from cytokine-induced signalling by modulation of JH2 αC helix. *Biochem. J.* **473**, 1579–1591 (2016).
36. A. Dusa, C. Mouton, C. Pecquet, M. Herman, S. N. Constantinescu, JAK2 V617F constitutive activation requires JH2 residue F595: A pseudokinase domain target for specific inhibitors. *PLOS ONE* **5**, e11157 (2010).
37. J. Raivola, T. Haikarainen, O. Silvennoinen, Characterization of JAK1 pseudokinase domain in cytokine signaling. *Cancers* **12**, 78 (2020).
38. M. S. Valdés-Tresanco, M. E. Valdés-Tresanco, P. A. Valiente, E. Moreno, gmx_MMPBSA: A new tool to perform end-state free energy calculations with GROMACS. *J. Chem. Theory Comput.* **17**, 6281–6291 (2021).
39. S. M. Hoy, Deucravacitinib: First approval. *Drugs* **82**, 1671–1679 (2022).
40. H. M. Hammarén, D. Ungureanu, J. Grisouard, R. C. Skoda, S. R. Hubbard, O. Silvennoinen, ATP binding to the pseudokinase domain of JAK2 is critical for pathogenic activation. *Proc. Natl. Acad. Sci. U.S.A.* **112**, 4642–4647 (2015).

41. R. D. Ferrao, H. J. Wallweber, P. J. Lupardus, Receptor-mediated dimerization of JAK2 FERM domains is required for JAK2 activation. *eLife* **7** (2018).
42. O. Livnah, E. A. Stura, D. L. Johnson, S. A. Middleton, L. S. Mulcahy, N. C. Wrighton, W. J. Dower, L. K. Jolliffe, I. A. Wilson, Functional mimicry of a protein hormone by a peptide agonist: The EPO receptor complex at 2.8 Å. *Science* **273**, 464–471 (1996).
43. R. S. Syed, S. W. Reid, C. Li, J. C. Cheetham, K. H. Aoki, B. Liu, H. Zhan, T. D. Osslund, A. J. Chirino, J. Zhang, J. Finer-Moore, S. Elliott, K. Sitney, B. A. Katz, D. J. Matthews, J. J. Wendoloski, J. Egrie, R. M. Stroud, Efficiency of signalling through cytokine receptors depends critically on receptor orientation. *Nature* **395**, 511–516 (1998).
44. I. Remy, I. A. Wilson, S. W. Michnick, Erythropoietin receptor activation by a ligand-induced conformation change. *Science* **283**, 990–993 (1999).
45. S. N. Constantinescu, T. Keren, M. Socolovsky, H. Nam, Y. I. Henis, H. F. Lodish, Ligand-independent oligomerization of cell-surface erythropoietin receptor is mediated by the transmembrane domain. *Proc. Natl. Acad. Sci. U.S.A.* **98**, 4379–4384 (2001).
46. M. S. P. Corbett, A. E. Mark, D. Poger, Do all x-ray structures of protein-ligand complexes represent functional states? EPOR, a case study. *Biophys. J.* **112**, 595–604 (2017).
47. S. R. Hubbard, Mechanistic insights into regulation of JAK2 tyrosine kinase. *Front. Endocrinol.* **8**, 361 (2018).
48. M. Atanasova, A. Whitty, Understanding cytokine and growth factor receptor activation mechanisms. *Crit. Rev. Biochem. Mol. Biol.* **47**, 502–530 (2012).
49. J. J. Babon, I. S. Lucet, J. M. Murphy, N. A. Nicola, L. N. Varghese, The molecular regulation of Janus kinase (JAK) activation. *Biochem. J.* **462**, 1–13 (2014).
50. T. N. Baldering, J. T. Bullerjahn, G. Hummer, M. Heilemann, S. Malkusch, Molecule counts in complex oligomers with single-molecule localization microscopy. *J. Phys. D Appl. Phys.* **52**, 474002 (2019).

51. A. J. Brooks, W. Dai, M. L. O'Mara, D. Abankwa, Y. Chhabra, R. A. Pelekanos, O. Gardon, K. A. Tunney, K. M. Blucher, C. J. Morton, M. W. Parker, E. Sierecki, Y. Gambin, G. A. Gomez, K. Alexandrov, I. A. Wilson, M. Doxastakis, A. E. Mark, M. J. Waters, Mechanism of activation of protein kinase JAK2 by the growth hormone receptor. *Science* **344**, 1249783 (2014).
52. H. Yao, Y. Ma, Z. Hong, L. Zhao, S. A. Monaghan, M.-C. Hu, L. J. Huang, Activating JAK2 mutants reveal cytokine receptor coupling differences that impact outcomes in myeloproliferative neoplasm. *Leukemia* **31**, 2122–2131 (2017).
53. J. Grisouard, S. Li, L. Kubovcakova, T. N. Rao, S. C. Meyer, P. Lundberg, H. Hao-Shen, V. Romanet, M. Murakami, T. Radimerski, S. Dirnhofer, R. C. Skoda, JAK2 exon 12 mutant mice display isolated erythrocytosis and changes in iron metabolism favoring increased erythropoiesis. *Blood* **128**, 839–851 (2016).
54. C. Haan, C. Rolvering, F. Raulf, M. Kapp, P. Drückes, G. Thoma, I. Behrmann, H.-G. Zerwes, Jak1 has a dominant role over Jak3 in signal transduction through γ c-containing cytokine receptors. *Chem. Biol.* **18**, 314–323 (2011).
55. F. Kohlhuber, N. C. Rogers, D. Watling, J. Feng, D. Guschin, J. Briscoe, B. A. Witthuhn, S. V. Kotenko, S. Pestka, G. R. Stark, J. N. Ihle, I. M. Kerr, A JAK1/JAK2 chimera can sustain α and γ interferon responses. *Mol. Cell. Biol.* **17**, 695–706 (1997).
56. G. Hummer, F. Fricke, M. Heilemann, Model-independent counting of molecules in single-molecule localization microscopy. *Mol. Biol. Cell* **27**, 3637–3644 (2016).
57. C. Krüger, F. Fricke, C. Karathanasis, M. S. Dietz, S. Malkusch, G. Hummer, M. Heilemann, Molecular counting of membrane receptor subunits with single-molecule localization microscopy. *Proc. SPIE* **10071**, 100710K (2017).
58. M. Ovesný, P. Křížek, J. Borkovec, Z. Svindrych, G. M. Hagen, ThunderSTORM: A comprehensive ImageJ plug-in for PALM and STORM data analysis and super-resolution imaging. *Bioinformatics* **30**, 2389–2390 (2014).

59. S. Malkusch, M. Heilemann, Extracting quantitative information from single-molecule super-resolution imaging data with LAMA—Localization microscopy analyzer. *Sci. Rep.* **6**, 34486 (2016).
60. C. Leterrier, J. Potier, G. Caillol, C. Debarnot, F. Rueda Boroni, B. Dargent, Nanoscale architecture of the axon initial segment reveals an organized and robust scaffold. *Cell Rep.* **13**, 2781–2793 (2015).
61. P. I. Bastiaens, I. V. Majoul, P. J. Verveer, H. D. Söling, T. M. Jovin, Imaging the intracellular trafficking and state of the AB5 quaternary structure of cholera toxin. *EMBO J.* **15**, 4246–4253 (1996).
62. J. Schindelin, I. Arganda-Carreras, E. Frise, V. Kaynig, M. Longair, T. Pietzsch, S. Preibisch, C. Rueden, S. Saalfeld, B. Schmid, J.-Y. Tinevez, D. J. White, V. Hartenstein, K. Eliceiri, P. Tomancak, A. Cardona, Fiji: An open-source platform for biological-image analysis. *Nat. Methods* **9**, 676–682 (2012).
63. A. T. Virtanen, T. Haikarainen, P. Sampathkumar, M. Palmroth, S. Liukkonen, J. Liu, N. Nekhotiaeva, S. R. Hubbard, O. Silvennoinen, Identification of novel small molecule ligands for JAK2 pseudokinase domain. *Pharmaceuticals* **16**, 75 (2023).
64. W. Kabsch, XDS. *Acta Crystallogr. D. Biol. Crystallogr.* **66**, 125–132 (2010).
65. R. M. Bandaranayake, D. Ungureanu, Y. Shan, D. E. Shaw, O. Silvennoinen, S. R. Hubbard, Crystal structures of the JAK2 pseudokinase domain and the pathogenic mutant V617F. *Nat. Struct. Mol. Biol.* **19**, 754–759 (2012).
66. D. Liebschner, P. V. Afonine, M. L. Baker, G. Bunkóczki, V. B. Chen, T. I. Croll, B. Hintze, L.-W. Hung, S. Jain, A. J. McCoy, N. W. Moriarty, R. D. Oeffner, B. K. Poon, M. G. Prisant, R. J. Read, J. S. Richardson, D. C. Richardson, M. D. Sammito, O. V. Sobolev, D. H. Stockwell, T. C. Terwilliger, A. G. Urzhumtsev, L. L. Videau, C. J. Williams, P. D. Adams, Macromolecular structure determination using X-rays, neutrons and electrons: Recent developments in Phenix. *Acta Crystallogr. D. Struct. Biol.* **75**, 861–877 (2019).

67. P. Emsley, B. Lohkamp, W. G. Scott, K. Cowtan, Features and development of Coot. *Acta Crystallogr. D Biol. Crystallogr.* **66**, 486–501 (2010).
68. R. McNally, Q. Li, K. Li, C. Dekker, E. Vangrevelinghe, M. Jones, P. Chène, R. Machauer, T. Radimerski, M. J. Eck, Discovery and structural characterization of ATP-site ligands for the wild-type and V617F mutant JAK2 pseudokinase domain. *ACS Chem. Biol.* **14**, 587–593 (2019).
69. J. Huang, S. Rauscher, G. Nawrocki, T. Ran, M. Feig, B. L. de Groot, H. Grubmüller, A. D. MacKerell, CHARMM36m: An improved force field for folded and intrinsically disordered proteins. *Nat. Methods* **14**, 71–73 (2017).
70. W. L. Jorgensen, J. Chandrasekhar, J. D. Madura, R. W. Impey, M. L. Klein, Comparison of simple potential functions for simulating liquid water. *J. Chem. Phys.* **79**, 926–935 (1983).
71. M. J. Abraham, T. Murtola, R. Schulz, S. Páll, J. C. Smith, B. Hess, E. Lindahl, GROMACS: High performance molecular simulations through multi-level parallelism from laptops to supercomputers. *SoftwareX* **1-2**, 19–25 (2015).
72. B. Hess, H. Bekker, H. J. C. Berendsen, J. G. E. M. Fraaije, LINCS: A linear constraint solver for molecular simulations. *J. Comput. Chem.* **18**, 1463–1472 (1997).
73. T. Darden, D. York, L. Pedersen, Particle mesh Ewald: An $N \cdot \log(N)$ method for Ewald sums in large systems. *J. Chem. Phys.* **98**, 10089–10092 (1993).
74. W. G. Hoover, Canonical dynamics: Equilibrium phase-space distributions. *Phys. Rev. A. Gen. Phys.* **31**, 1695–1697 (1985).
75. S. Nosé, A unified formulation of the constant temperature molecular dynamics methods. *J. Chem. Phys.* **81**, 511–519 (1984).
76. M. Parrinello, A. Rahman, Polymorphic transitions in single crystals: A new molecular dynamics method. *J. Appl. Phys.* **52**, 7182–7190 (1981).

77. J. S. Hub, B. L. de Groot, D. van der Spoel, g_wham—A free weighted histogram analysis implementation including robust error and autocorrelation estimates. *J. Chem. Theory Comput.* **6**, 3713–3720 (2010).
78. S. Kumar, J. M. Rosenberg, D. Bouzida, R. H. Swendsen, P. A. Kollman, The weighted histogram analysis method for free-energy calculations on biomolecules. I. The method. *J. Comput. Chem.* **13**, 1011–1021 (1992).
79. A. Onufriev, D. Bashford, D. A. Case, Exploring protein native states and large-scale conformational changes with a modified generalized born model. *Proteins* **55**, 383–394 (2004).
80. J. Jumper, R. Evans, A. Pritzel, T. Green, M. Figurnov, O. Ronneberger, K. Tunyasuvunakool, R. Bates, A. Žídek, A. Potapenko, A. Bridgland, C. Meyer, S. A. A. Kohl, A. J. Ballard, A. Cowie, B. Romera-Paredes, S. Nikolov, R. Jain, J. Adler, T. Back, S. Petersen, D. Reiman, E. Clancy, M. Zielinski, M. Steinegger, M. Pacholska, T. Berghammer, S. Bodenstein, D. Silver, O. Vinyals, A. W. Senior, K. Kavukcuoglu, P. Kohli, D. Hassabis, Highly accurate protein structure prediction with AlphaFold. *Nature* **596**, 583–589 (2021).
81. M. Varadi, S. Anyango, M. Deshpande, S. Nair, C. Natassia, G. Yordanova, D. Yuan, O. Stroe, G. Wood, A. Laydon, A. Žídek, T. Green, K. Tunyasuvunakool, S. Petersen, J. Jumper, E. Clancy, R. Green, A. Vora, M. Lutfi, M. Figurnov, A. Cowie, N. Hobbs, P. Kohli, G. Kleywegt, E. Birney, D. Hassabis, S. Velankar, AlphaFold Protein Structure Database: Massively expanding the structural coverage of protein-sequence space with high-accuracy models. *Nucleic Acids Res.* **50**, D439–D444 (2022).
82. S. Jo, T. Kim, V. G. Iyer, W. Im, CHARMM-GUI: A web-based graphical user interface for CHARMM. *J. Comput. Chem.* **29**, 1859–1865 (2008).
83. R. A. Laskowski, J. Jabłońska, L. Pravda, R. S. Vařeková, J. M. Thornton, PDBsum: Structural summaries of PDB entries. *Protein Sci.* **27**, 129–134 (2018).